Liquid drops and surface tension with smoothed particle applied mechanics

S. Nugent and H. A. Posch
Institut für Experimentalphysik, Universität Wien, Boltzmanngasse 5, A-1090 Wien, Austria
(Received 11 May 2000)

Smoothed particle applied mechanics (SPAM), also referred to as smoothed particle hydrodynamics, is a Lagrangian particle method for the simulation of continuous flows. Here we apply it to the formation of a liquid drop, surrounded by its vapor, for a van der Waals (vdW) fluid in two dimensions. The cohesive pressure of the vdW equation of state gives rise to an attractive, central force between the particles with an interaction range which is assumed to exceed the interaction range of all the other smoothed forces in the SPAM equations of motion. With this assumption, stable drops are formed, and the vdW phase diagram is well reproduced by the simulations. Below the critical temperature, the surface tension for equilibrated drops may be computed from the pressure excess in their centers. It agrees very well with the surface tension independently determined from the vibrational frequency of weakly excited drops. We also study strongly deformed drops performing large-amplitude oscillations, which are reminiscent of the oscillations of a large ball of water under microgravity conditions. In an appendix we comment on the limitations of SPAM by studying the violation of angular momentum conservation, which is a consequence of noncentral forces contributed by the full Newtonian viscous stress tensor.

PACS number(s): 47.11.+j, 47.55.Dz, 02.60.−x, 02.70.Ns

I. INTRODUCTION

For the simulation of continuous, multiphase flows, the incorporation of surface properties for the phase boundaries constitutes an interesting problem. In particular, many theoretical schemes have been put forward to treat surface tension for two-phase flows [1–3]. Here, we apply some of these ideas to a van der Waals (vdW) fluid exhibiting a liquid-gas phase transition below the critical point. We study the formation and the dynamics of a circular drop floating in its atmosphere, where we apply a Lagrangian particle method to integrate the continuous flow equations. Originally invented for astrophysical problems [4,5], the method is widely known as smoothed particle hydrodynamics (SPH). Because of its even wider applicability in continuum mechanics, we also refer to it as smoothed particle applied mechanics (SPAM) [6,7]. It has some advantages over standard grid-based and hybrid methods, and has comparable accuracy [8] and superior stability properties. It is easily extended to three dimensions and may be adapted to include external driving fields. As a disadvantage, the method may sometimes be somewhat more expensive computationally than conventional grid-based algorithms.

In SPAM (or SPH) the continuous flow, at time t, is represented by a set of ''particles'' located at $\mathbf{r}_i(t)$ and moving with velocity $\mathbf{v}_i(t)$, $i=1,\ldots,N$. In addition to their mass m_i, the particles carry field properties such as the mass density ρ_i and the internal energy per unit mass, u_i. The ''smoothed'' value of any field function $f(\mathbf{r},\mathbf{v})$ at a space point $\mathbf{r}$ is a weighted sum of all contributions from neighboring particles [5,9],

$$\langle f(\mathbf{r},\mathbf{v})\rangle=\sum_{j=1}^{N}\frac{m_j}{\rho(\mathbf{r}_j)}f(\mathbf{r}_j,\mathbf{v}_j)w(|\mathbf{r}-\mathbf{r}_j|,h), \tag{1}$$

and its gradient becomes

$$\langle\nabla f(\mathbf{r},\mathbf{v})\rangle=\sum_{j=1}^{N}\frac{m_j}{\rho(\mathbf{r}_j)}f(\mathbf{r}_j,\mathbf{v}_j)\nabla w(|\mathbf{r}-\mathbf{r}_j|,h). \tag{2}$$

The weight or smoothing function $w(|\mathbf{r}|,h)$ is assumed to be an even function of finite range $h>0$, which vanishes smoothly for $|\mathbf{r}|\equiv r\geqslant h$, and which is normalized to unity when integrated over space. The interpolated function $\langle f\rangle$ agrees with the true field function f up to $O(h^2)+\epsilon_N$, where the particle error ϵ_N depends on the distribution of the particles and is minimal for regular crystal-like structures [10,11]. To the same order of approximation, $\langle fg\rangle=\langle f\rangle\langle g\rangle+O(h^2)$ for field functions f and g. Since there is no danger for misinterpretation, we drop the brackets for the interpolated functions in the following. With the discretized summation interpolant for f and ∇f, the partial differential equations of continuum mechanics are converted into a set of ordinary differential equations for $\mathbf{r}_i(t)$ and $\mathbf{v}_i(t)$ reminiscent of conventional molecular dynamics. For an inviscid flow of a two-dimensional adiabatic ideal gas in the bulk, SPAM is even isomorphic to molecular dynamics with $w(r)$ taking the role of the pair potential [12]. Interestingly, there is also a close link between the smoothed particles and the embedded atoms used for the simulation of metals [13].

The smoothed-particle representation of the equations of motion is not unique. For completeness, we summarize in Sec. II the equations used in this study [7,14]. We show how to apply them to a vdW fluid in two dimensions. In Sec. III we discuss the equilibrium properties of circular drops and show that the simulations closely reproduce the phase diagram of a vdW fluid away from the critical region. The surface tension is computed from the Laplace equation, which relates the excess pressure in the center of a drop to the curvature of the drop surface. In Sec. IV we demonstrate the application of smoothed-particle simulations to the study of

drop vibrations. The surface tension obtained from the vibrational frequency agrees very well with the Laplace-equation result for equilibrated drops.

The particle interactions in SPAM are generally noncentral due to the Newtonian viscous stress in the equations of motion. It follows that angular momentum is not conserved as is required by continuum mechanics, but decreases exponentially in time with a decay time proportional to $1/h^2$. This error of order $O(h^2)$ is investigated in the Appendix by simulating the dynamics of rotating circular drops in two dimensions.

II. THE SPAM EQUATIONS OF MOTION FOR THE van der WAALS FLUID

In the first step, the mass density ρ_i of the particles is computed from

$$\rho_i = \sum_{j=1}^{N} m_j w_{ij}^h, \quad w_{ij}^h \equiv w(|\mathbf{r}_i - \mathbf{r}_j|, h), \tag{3}$$

where m_i is the mass of particle i. As always with SPAM, sums over particles include also the self-term for which $i=j$. Equation (3) conserves the total mass. For the SPAM equations of motion we use a representation that contains the full Newtonian viscous stress tensor and Fourier's heat flux vector as described in Refs. [7,14,15],

$$\frac{d\mathbf{r}_i}{dt} = \mathbf{v}_i,$$

$$\frac{d\mathbf{v}_i}{dt} = -\sum_{j=1}^{N} m_j \left(\frac{\mathbf{P}_i}{\rho_i^2} + \frac{\mathbf{P}_j}{\rho_j^2} \right) \cdot \nabla w_{ij}^h, \tag{4}$$

$$\frac{du_i}{dt} = \frac{1}{2} \sum_{j=1}^{N} m_j \left(\frac{\mathbf{P}_i}{\rho_i^2} + \frac{\mathbf{P}_j}{\rho_j^2} \right) : (\mathbf{v}_i - \mathbf{v}_j) \nabla_i w_{ij}^h - \sum_{j=1}^{N} m_j \left(\frac{\mathbf{Q}_i}{\rho_i^2} + \frac{\mathbf{Q}_j}{\rho_j^2} \right) \cdot \nabla_i w_{ij}^h. \tag{5}$$

In these equations, u_i is the internal energy per unit mass, $\mathbf{P}_i$ is the pressure tensor, and $\mathbf{Q}_i$ is the heat flux vector, all computed at the position of particle i. As mentioned before, these equations are not unique and depend on the particular implementation of various field gradients into the SPAM scheme. They have already been shown to give good results for a variety of bulk flows [6,7,14,15].

The equilibrium and transport properties of the material enter through the pressure tensor $\mathbf{P}_i$ and the heat flux vector $\mathbf{Q}_i$. Formally,

$$\mathbf{P}_i = p_i \mathbf{1} - \boldsymbol{\sigma}_i - \eta_v (\nabla \cdot \mathbf{v})_i \mathbf{1}, \tag{6}$$

$$\boldsymbol{\sigma}_i = \eta \left[\nabla \mathbf{v} + \nabla \mathbf{v}^+ - \frac{2}{d} (\nabla \cdot \mathbf{v}) \mathbf{1} \right]_i, \tag{7}$$

where the velocity gradient tensor in the SPAM representation is given by

$$(\nabla \mathbf{v})_i = m \sum_{j=1}^{N} \frac{\mathbf{v}_j - \mathbf{v}_i}{\rho_{ij}} \nabla w_{ij}^h. \tag{8}$$

In these equations, p_i is the pressure, and $\boldsymbol{\sigma}_i$ is the Newtonian shear stress tensor, all evaluated at the position of particle i. η and η_v denote the shear and bulk viscosities, respectively, and $d=2$ is the spatial dimension. The notation $^+$ means transposition, and $\mathbf{1}$ denotes a unit tensor. Similarly, from Fourier's law of heat conduction one has

$$\mathbf{Q}_i = -\kappa (\nabla T)_i, \tag{9}$$

where the SPAM representation of the temperature gradient is written as

$$(\nabla T)_i = m \sum_{j=1}^{N} \frac{T_j - T_i}{\rho_{ij}} \nabla_i w_{ij}^h. \tag{10}$$

Here, T_i is the temperature associated with i, and κ is the heat conductivity. Furthermore, $\rho_{ij} \equiv (\rho_i + \rho_j)/2$.

In the following we restrict ourselves to two dimensions, $d=2$, and the two-dimensional version of the weight function introduced by Lucy [4,7] is used,

$$w(r,h) = \begin{cases} \dfrac{5}{\pi h^2} \left(1 + \dfrac{3r}{h} \right) \left(1 - \dfrac{r}{h} \right)^3 & \text{if } r < h \\ 0 \quad \text{if } r \geqslant h, \end{cases} \tag{11}$$

which is a quartic spline. Other smoothing functions, such as cubic or quintic splines [3], have been examined by other authors.

The shear stress tensor $\boldsymbol{\sigma}$ is symmetric, of second rank, and proportional to the shear viscosity η. The viscous forces contributed by $\boldsymbol{\sigma}$ are noncentral forces in Eq. (4) and violate the conservation law for the total angular momentum $\mathbf{L}$. We shall come back to this point in the Appendix.

These equations are closed by the mechanical and caloric equations of state for the pressure p and the internal energy per unit mass, u, respectively. We consider the van der Waals model [16], which is simple enough to be derived from statistical mechanics, but still so realistic as to display a gas-to-liquid phase transition similar to that of a real fluid. The equations of state are obtained as the mean-field limit for the free energy density of a system of hard particles with a diameter σ and with a superimposed long-range, attractive, pair potential [17]. In terms of the mass density ρ (instead of the more familiar particle density) one has for the pressure p and for the internal energy per unit mass u,

$$p = \frac{\rho \bar{k} T}{1 - \rho \bar{b}} - \bar{a} \rho^2, \tag{12}$$

$$u = \bar{k} T - \rho \bar{a}. \tag{13}$$

In these equations, $\bar{k} \equiv k_B/m$, where k_B is the Boltzmann's constant, and m is the particle mass. Furthermore, $\bar{a} \equiv a/m^2$ and $\bar{b} \equiv b/m$ are, in essence, the familiar vdW parameters a

and b. a controls the strength of the attractive force, and $b = \sigma^2\pi/2$ is equal to twice the size of a disk (in two dimensions).

It is useful to consider the cohesive pressure, $-\overline{a}\rho^2$, separately. If this term, which contributes to **P**, is inserted into Eq. (4), one obtains for the corresponding acceleration

$$\left(\frac{d\mathbf{v}_i}{dt}\right)_a = 2\overline{a}\sum_j m_j \nabla_i w_{ij}^H. \tag{14}$$

This shows how the attractive, long-range, interatomic vdW forces are transformed into similarly attractive forces between the SPAM particles. The distance dependence of this force is determined by the smoothing function w. For reasons which will become clear below, we have denoted the smoothing range by H instead of h. The analogous contribution to the energy equation becomes

$$\left(\frac{du_i}{dt}\right)_a = -2\overline{a}\sum_{j=1}^{N} m_j(\mathbf{v}_i - \mathbf{v}_j)\cdot\nabla_i w_{ij}^H. \tag{15}$$

On the atomistic level, the attractive vdW forces give rise to a surface tension γ [18] which, until very recently, resisted theoretical prediction without severe approximations. Hadjiconstantinou *et al.* [19] were able to compute γ for this model with a modified direct-simulation Monte Carlo technique. On the level of continuum mechanics, Eq. (14) provides a simple volume force for the SPAM flow of a vdW fluid, which is expected to account for the formation of coexisting liquid and gaseous domains. At the same time, it generates the proper surface tension at the surfaces without the need of locating the surface and of determining its local curvature [3]. The surface tension is no input parameter of the simulation. Interestingly, Eq. (14) resembles the method used for the construction of normal vectors for smoothed surfaces with the help of a color function [1,5]. The forces represented by Eq. (14) largely cancel in the bulk, both liquid and gaseous, with small fluctuations around the overall direction of the macroscopic density gradient. But in a small strip of width H around a phase boundary, the accelerations of a particle i due to Eq. (14) are basically perpendicular to the surface, pointing toward the dense phase. Similar volume forces for the simulation of two-phase SPAM flows with surface tension were previously introduced, on a more intuitive level, by Hunter [20] and Hoover *et al.* [6].

Unfortunately, this simple formulation of the SPAM equations of motion leads to instabilities, as will be shown in the next section. There is a simple, although computationally costly, way around this problem, which we take for the simulation of vdW drops.

III. SIMULATION OF van der WAALS DROPS

If, as indicated in the preceding section, the *same* smoothing length, $H=h$, is used for the weight function w in *all* the terms contributing to the full particle acceleration $d\mathbf{v}_i/dt$ in Eq. (4), we do not get sensible results. Although an originally homogeneous fluid phase separates into a liquid and a gaseous phase for subcritical temperatures, the particles tend to form an interface which cannot be penetrated by other particles. Furthermore, low temperatures may result in negative particle temperatures T_i, terminating the simulation. However, if we turn to the mean-field basis of the vdW model and *increase* the smoothing length for the attractive force in Eq. (14) due to the cohesive pressure to $H=2h$, keeping the smoothing length for all other terms contributing to Eqs. (4) and (5) at h, we obtain very stable and circular drops such as depicted in Fig. 1 [21]. A similar observation, for a simpler equation of state, has already been made by Hoover *et al.* [6]. Of course, the price that has to be paid for this modification is heavy: there are about four times as many particles within the interaction range, and the computational effort rises accordingly.

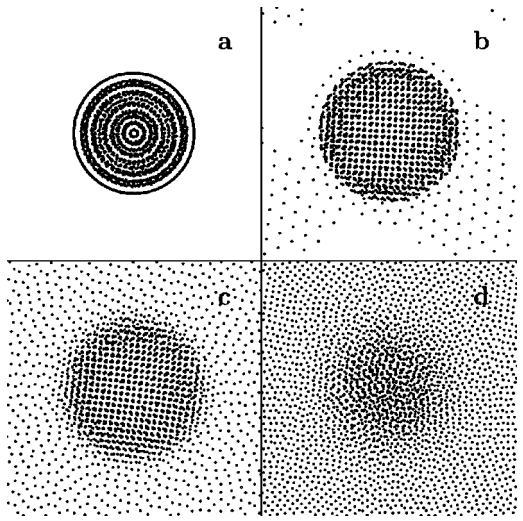

FIG. 1. Stable drop configurations for the reduced temperatures 0.2 (a), 0.6 (b), 0.87 (c), and 1.05 (d) of a vdW fluid. The critical temperature $T_c=1.19$ in our reduced units. $N=2500$ SPAM particles were used in a box of width $L=50$ with smoothing lengths amounting to $h=5$ and $H=10$. Equilibrium is not fully reached in (b).

In all simulations reported in this and the following section we take $N=2500$ smoothed particles of equal mass $m_i = m$. At time $t=0$ they are periodically arranged on a square, which is smaller than the square simulation box of width L. Periodic boundary conditions apply. We use reduced units for which $m=1$, $\overline{a}=2$, $\overline{b}=1/2$, and $\overline{k}=1$. In these units, the critical point of the vdW fluid [22] occurs for $T_c=32/27$, $\rho_c=2/3$, and $p_c=8/27$. We take $\eta=1$ and $\eta_v = 0.1$ for the shear and bulk viscosities, respectively, and $\kappa = 5$ for the heat conductivity. A fourth-order Runge-Kutta algorithm is used for the integration of the SPAM equations of motion. For most simulations, the time step $\Delta t=0.05$.

For a box of width $L=50$ and with periodic boundary conditions, we show typical equilibrated drops for various temperatures below T_c in Fig. 1. The smoothing lengths are $h=5$ and $H=10$.

The radial dependence of the temperature $T(r)$, of the density $\rho(r)$, and of the pressure $p(r)$, may be interpolated from an instantaneous configuration according to Eq. (1), where r is the distance from the center of mass. As an example, we show in Figs. 2, 3, and 4 the results for a drop with a temperature $T\approx 0.91$. From Fig. 2 we infer that the local temperatures at the drop center and in the surrounding vapor are nearly the same. This indicates that the drop is very close to thermal equilibrium. The spurious temperature de-

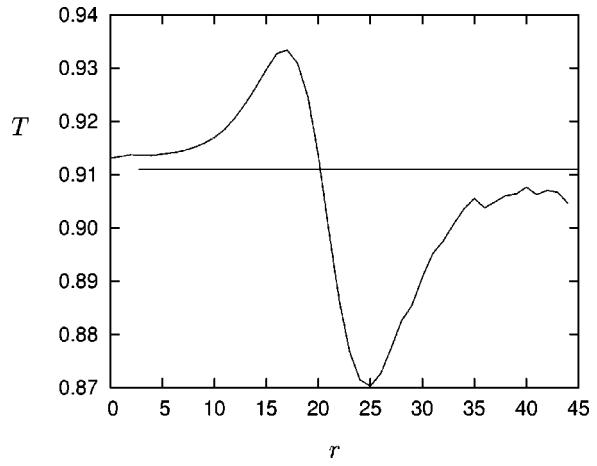

FIG. 2. SPAM-averaged radial temperature dependence $T(r)$, where r is the distance from the center of mass. All quantities are given in reduced units introduced in Sec. III.

viations from the mean in the figure are not present in the unsmoothed T_i associated with the individual particles. The positive and negative deviations are correlated with negative and positive curvatures, respectively, of the density profile in Fig. 3. They are a deficiency of the finite interpolation scheme of Eq. (1), which is second-order accurate in the smoothing length h. They may be reduced by reducing h. The penalty, of course, is an unavoidable increase of N for the description of the same flow.

The very pronounced minimum and maximum of the local pressure in Fig. 4 are a consequence of the vdW loops displayed by the isotherms of Eq. (12) for subcritical temperatures. They deviate from the flat tie-line obtained from Maxwell's equal-area rule [22]. The unstable states represented by these loops are not realized in the bulk, but they play a decisive role in the surface region separating the liquid from the vapor [18]. If one moves from the inside of a drop (with nonvanishing curvature) to its outside, one first passes through a layer of overheated liquid with negative pressure differences with respect to the Maxwell tie-line pressure, followed by a layer of undercooled vapor with positive pressure deviations, before entering the vapor phase. The ensuing integrated pressure contribution of the surface

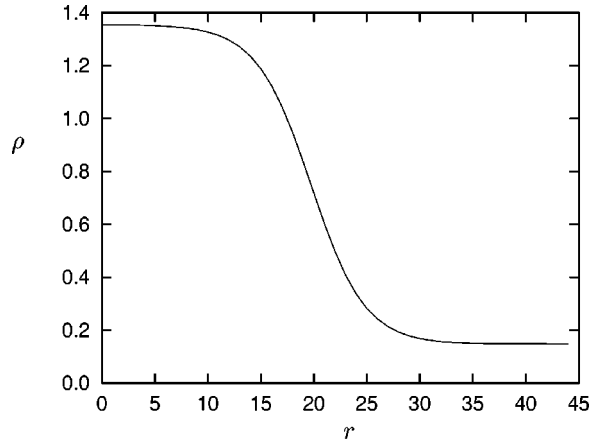

FIG. 3. SPAM-averaged radial mass-density dependence $\rho(r)$, where r is the distance from the center of mass. All quantities are given in reduced units introduced in Sec. III.

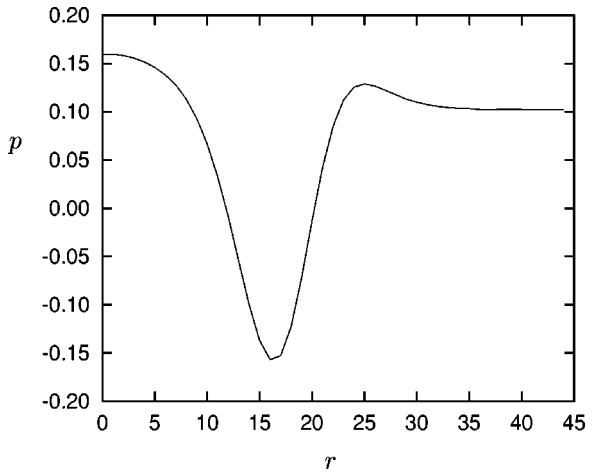

FIG. 4. SPAM-averaged radial pressure dependence $p(r)$, where r is the distance from the center of mass. All quantities are given in reduced units introduced in Sec. III.

layer gives rise to the surface tension γ. Condensation takes place such that in equilibrium the negative pressure is balanced by $p(0)-p(\infty)>0$ leading up to the Laplace equation [18]

$$p_l = p_g + \frac{\gamma}{R}. \tag{16}$$

It relates γ to the pressure in the drop center, $p_l \equiv p(0)$, and to the vapor pressure $p_g \equiv p(\infty)$ far away from the drop, and R is the radius for the equimolar surface of the drop. If the vdW loops are replaced by a flat tie line, the surface tension vanishes and no phase separation takes place in a simulation. Similar observations have been made before [19]. It is interesting to note that the unstable parts of the vdW equation are obtained by microcanonical molecular dynamics simulations of (relatively small) homogeneous bulk systems with periodic boundaries [23].

In Fig. 5 the phase diagram of the vdW fluid is shown.

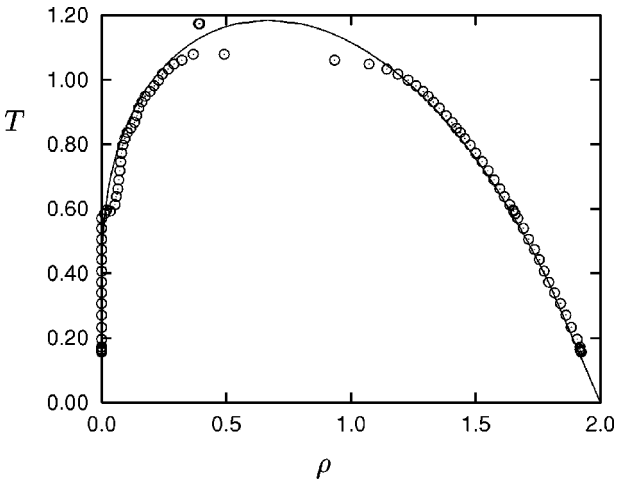

FIG. 5. Phase diagram $T(\rho)$ for the vdW fluid. The smooth line is the theoretical prediction, and the symbols are SPAM results. 2500 SPAM particles were used in a box of width $L=50$ with smoothing lengths amounting to $h=5$ and $H=10$. Reduced units are used which are defined in Sec. III.

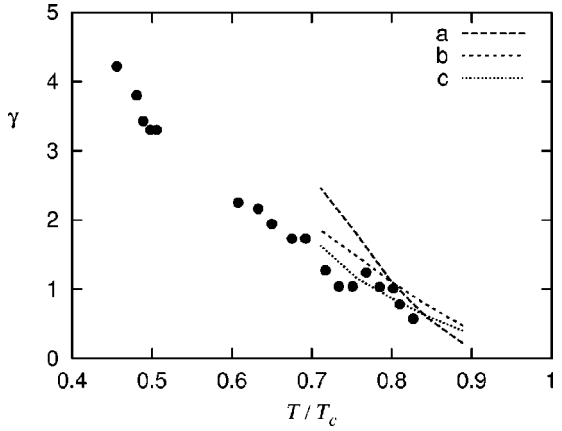

FIG. 6. Temperature dependence of the surface tension γ for the two-dimensional vdW fluid. $T_c = 32/27$ is the vdW critical temperature. Our reduced units are defined in the main text. The full dots are our SPAM results; the smooth lines refer to results of Ref. [19], where the labels *a*, *b*, and *c* distinguish between different methods of estimating γ. The estimated accuracy of all data is $\pm 15\%$. Reduced units are used which are defined in Sec. III.

The symbols refer to the SPAM results and are obtained from the densities and temperatures at the drop center and in the vapor far away from the drop. The theoretical prediction of Eq. (12), shown by the smooth line, are reproduced rather well, with two exceptions. First, in the critical region smoothing lengths $H=10$ and $h=5$, in combination with only 2500 SPAM particles in a box of width $L=50$, lead to a rather poorly defined drop such as depicted in Fig. 1(d). A reduction of H and h leads to less-smoothed drop boundaries and an improved equilibrium temperature. Second, the deviations of the vapor densities at low temperatures are inherent to the SPAM interpolation scheme. There are not enough neighboring SPAM particles within a circle of radius h to give a good representation of the local density. For $0.60 < T < 0.75$, the gas pressure is already so small that equilibrium is not fully reached within our simulation time. For $T < 0.6$, all SPAM particles are condensed and none remain in the vapor phase [as in Fig. 1(a)]. A remedy is again an (unfortunately expensive) increase of the number of particles.

We may verify from Fig. 3 that the largest smoothing length, $H=10$ in our case, determines the spatial resolution of the drop surface. The experimental profile is a convolution of the actual density profile with the smoothing function $w(r,h)$. It is difficult to extract the surface tension γ from the slope of $\rho(r)$ [18] at the equimolar surface, which divides the liquid from the ambient vapor. It is easier to compute γ directly from the Laplace equation (16). In two dimensions, the equimolar radius is given by

$$R^2 = \frac{2}{\rho_l - \rho_g}\int_0^\infty [\rho(r) - \rho_g] r\,dr = -\frac{1}{\rho_l - \rho_g}\int_0^\infty r^2 \frac{d\rho}{dr}\,dr, \tag{17}$$

where $\rho(r)$ is the density profile as in Fig. 3, and $\rho_l \equiv \rho(0)$, $\rho_g \equiv \rho(\infty)$. Using the first equality of Eq. (17) for the computation of R, we show in Fig. 6 the surface tension for the two-dimensional vdW liquid as a function of temperature (full dots). The estimated uncertainty for these data is $\pm 15\%$. We have excluded the temperature range for which the numerical vapor density deviates significantly from the vdW theory in the phase diagram of Fig. 5.

These data may be compared to the direct simulation Monte Carlo results of Ref. [19], which were obtained for a three-dimensional system, but with a very shallow rectangular simulation box of extension $54.6\sigma \times 54.6\sigma \times 2.7\sigma$. σ is the vdW hard-core radius. Since the range of the attractive vdW force is expected to exceed the third box dimension, we may reinterpret their pressure as a normal force per unit length in two dimensions. Converted to our reduced units, the results of Ref. [19] are shown as smooth lines in Fig. 6. They are based on three independent methods of estimating γ: (a) is from the Laplace equation, (b) makes use of a mechanical method due to Elsner [24], and (c) is obtained from the Gibbs free energy excess per unit volume and the density gradient at the drop interface for the vdW fluid [18]. If we consider that also these data have an uncertainty comparable to that of our results, the comparison in Fig. 6 is rather successful.

IV. OSCILLATING van der WAALS DROPS

Next, we study excited vdW drops performing small-amplitude oscillations. From the period τ an independent estimate of the surface tension γ_τ is obtained. As is shown below, it is in excellent agreement with γ from the Laplace equation (16) for the circular drop in equilibrium.

To prove this assertion, we take as a starting point a well-equilibrated circular drop of 2500 SPAM particles, with density $\rho_l = 1.69$, equimolar radius $R=22.2$, and a rather low temperature, $T=0.54$. It looks similar to that in Fig. 1(a), with no particles remaining in the vapor phase ($p_g = 0$). Since $p_l - p_g = 0.19$ for this drop, the Laplace equation (16) yields $\gamma = 4.2$.

Next, this drop is converted into an elliptic drop with eccentricity $e=0.55$ and the major axes aligned along the y axis. This is achieved with an area-preserving and, hence, density-conserving transformation for the particle coordinates,

$$\begin{pmatrix} x' \\ y' \end{pmatrix} = \sqrt{\frac{2}{\sin\phi}}\, r \begin{pmatrix} \sin(\phi/2)\sin u \\ \cos(\phi/2)\cos u \end{pmatrix}, \tag{18}$$

where $r = \sqrt{x^2+y^2}$, $u = \arctan(x/y)$, and $\phi = e\pi$. For the viscosities we take $\eta = \eta_v = 0$, and for the heat conductivity $\kappa = 5$. This large value for κ serves to obtain fast temperature adjustment, reducing density fluctuations in the drop. When released, the time evolution of the maximum drop extension in x and y directions is shown in Fig. 7. It conforms to a damped oscillation with period $\tau = 168$. The damping is due to the finite heat conductivity, and, to a large extent, to the intrinsic viscosity, which is inherent to particle systems [7] and is effective in spite of a vanishing η.

For small vibration amplitudes, a theory by Lord Rayleigh [25] may be used to relate the period τ to the surface tension. In Ref. [25] the surface energy per unit length of an infinitely extended, cylindrical fluid is used for the computation of the eigenfrequencies of the cylinder, where the fluid is assumed to be inviscid and incompressible. Restricting this three-dimensional result to our two-dimensional drops (by taking $n=2$ and $k=0$ in Ref. [25]), one obtains

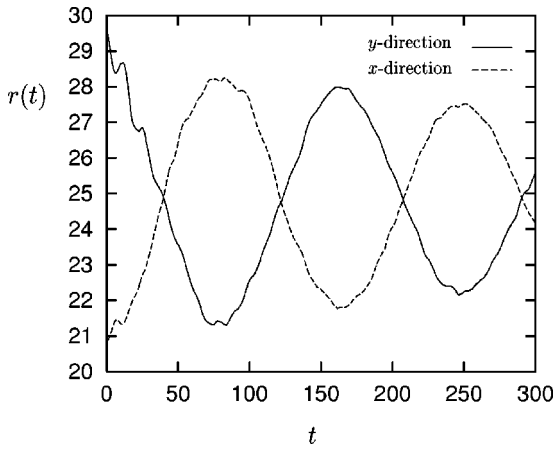

FIG. 7. Small-amplitude oscillations of the extension of a vdW drop along the x and y axes, initially prepared with an elliptical shape aligned with the frame of reference. The shear viscosity $\eta=0$, the bulk viscosity $\eta_v=0$, and the heat conductivity $\kappa=5$.

$$\tau=2\pi\sqrt{\frac{R^3\rho}{6\gamma}}. \tag{19}$$

From $\tau=168$ we find $\gamma_\tau=4.1$ in excellent agreement with γ. This shows that small-amplitude oscillations of drops are well reproduced by the SPAM simulations if performed consistently [26].

Also very large amplitude oscillations may be studied successfully. In Fig. 8 we show a sequence of snapshots for a drop, which was initially prepared by slowly deforming the same circular drop as before along the y axis with two reflecting pistons, until an aspect ratio of about 5 is reached. When released, this drop carries out vibrations that closely resemble the oscillations observed experimentally for a large ball of water under microgravity conditions in the space shuttle Columbia [27].

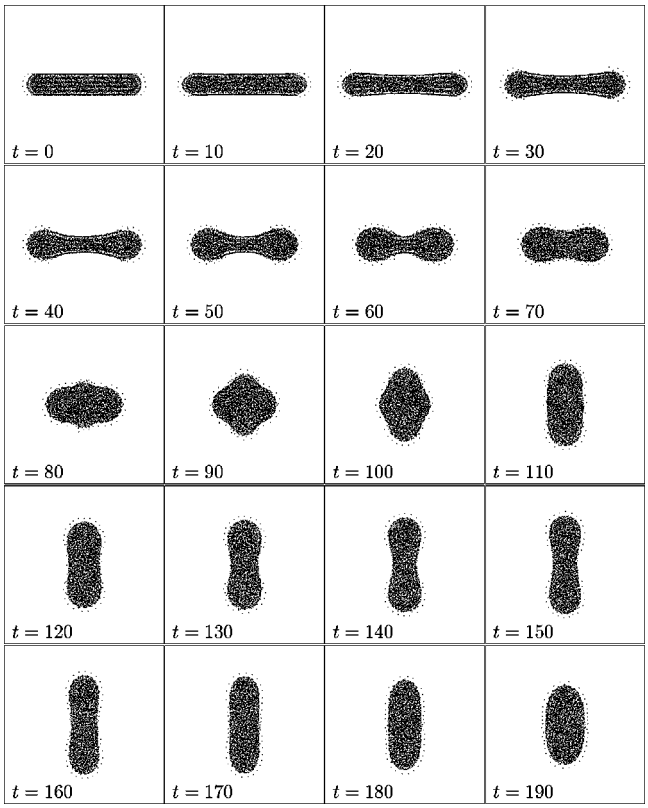

FIG. 8. Snapshots of the large-amplitude oscillations of a two-dimensional vdW drop with an initial aspect ratio close to 5 for various times t. All quantities are given in reduced units introduced in the main text.

V. CONCLUSIONS

We show in this paper that the smoothed-particle method may easily be adapted to studying two-phase flows and drop condensation for a van der Waals fluid. The vdW cohesive pressure $-a\rho^2$ gives rise to an attractive, central force acting between the smoothed particles. These forces are expected to cancel each other in the bulk and to be effective only in the neighborhood of a phase boundary. Their interaction range H needs to be larger than h, the interaction range of all other forces entering the SPAM equations of motion, to remove the instability ensuing for $H=h$. Taking $H=2h$, we obtain very stable circular drops in two dimensions, and the phase diagram of the vdW fluid is closely reproduced. The surface tension may be determined from the Laplace equation (16).

By deforming a circular drop, the restoring force due to the surface tension leads to a damped oscillation when the drop is released. The damping is a consequence of both the intrinsic transport mechanisms inherent to any particle system, and the macroscopic parameters η, η_v, and κ explicitly entering the SPAM equations of motion. For small-amplitude vibrations, the surface tension obtained from the oscillation frequency agrees well with that from the Laplace equation for equilibrated drops.

ACKNOWLEDGMENTS

We have profited greatly from discussions with Bill Hoover and with Berni Alder, whom we also thank for a preprint of Ref. [19]. We gratefully acknowledge the financial support by the *Fonds zur Förderung der wissenschaftlichen Forschung*, Grant No. P11428-PHY.

APPENDIX

Here we study the violation of angular momentum conservation due to the noncentral forces contributed to Eq. (4) by the shear stress $\boldsymbol{\sigma}$. Let us consider the continuum limit first. If $\mathcal{V}$ is an arbitrary volume comoving with the fluid and with surface $\mathcal{O}$, the time derivative of its angular momentum,

$$\frac{d\mathbf{L}}{dt}=\frac{d}{dt}\int_{\mathcal{V}}\mathbf{r}\times\mathbf{v}\rho d^d\mathbf{r}, \tag{A1}$$

is easily converted into a surface integral on $\mathcal{O}$ [11,28]. As before, d is the dimension of space. For a conservative system fully contained within $\mathcal{O}$, this integral vanishes and the total angular momentum is conserved.

In the smooth-particle representation with finite N and $h>0$, the corresponding expression is

$$\frac{d\mathbf{L}}{dt} = m\sum_{i=1}^{N} \mathbf{r}_i \times \frac{d\mathbf{v}_i}{dt} = \frac{\eta m^2}{2} \sum_{i=1}^{N} \sum_{j>i}^{N} \mathbf{r}_{ij} \times \left(\frac{\boldsymbol{\sigma}_i}{\rho_i^2} + \frac{\boldsymbol{\sigma}_j}{\rho_j^2} \right) \frac{dw_{ij}^h}{dr_{ij}} \cdot \hat{\mathbf{r}}_{ij}, \tag{A2}$$

where we have used Eqs. (4) and (7). In this equation $\mathbf{r}_{ij} = \mathbf{r}_i - \mathbf{r}_j$, and the caret denotes a unit vector. All SPAM particles are given the same mass, m. Equation (A2) differs from the exact continuum expression (A1) by a term of order h^2 due to the interpolation errors for the velocity gradient tensor $\boldsymbol{\nabla}\mathbf{v}$ appearing in the shear stress tensor $\boldsymbol{\sigma}$.

In this appendix we take the equation of state of a two-dimensional, adiabatic ideal gas, augmented by a negative constant,

$$p \propto \rho^2 - A, \quad A > 0 \tag{A3}$$

which has already been demonstrated to provide phase separation with smoothed particles [6]. However, the surface pressure generated by the artificial constant $-A$ is not sufficient to guarantee the formation of *circular* drops once condensation has taken place and p has approached zero. Therefore, the equation of motion (4) is augmented by an additional term on the right-hand side,

$$\left(\frac{d\mathbf{v}_i}{dt} \right)_s = -\frac{sm}{h^2} \sum_{j=1}^{N} w_{ij}^H \mathbf{r}_{ij}, \tag{A4}$$

which serves the same purpose as Eq. (14) for the vdW fluid in Sec. III. Equation (A4) represents an *attractive* interparticle force controled by the parameter $s > 0$, which is assumed to be of longer range, $H = 2h$, than all the other terms in Eq. (4). Since it is a central force, it does not affect the decay properties of the total angular momentum. Its only purpose is to provide sufficient additional surface tension in combination with our simple equation of state. Since this force also affects the transport of energy, an equivalent term is added to the energy equation (5),

$$\left(\frac{du_i}{dt} \right)_s = \frac{sm}{2h^2} \sum_{j=1}^{N} w_{ij}^H (\mathbf{v}_i - \mathbf{v}_j) \cdot \mathbf{r}_{ij}. \tag{A5}$$

The scaling according to sm/h^2 is introduced to allow for the same value of the force parameter s, if h and N are varied.

For the following we use reduced units, for which the mechanical and thermal equations of state are $p = \rho^2 - 1$ and $u = \rho - (1/\rho) + \bar{k}T$, respectively. As in Sec. III, $\bar{k} \equiv k_B/m$ is set equal to unity and is independent of N. (The latter follows from the requirement that the total mass, Nm, and the total internal energy, $U \equiv \Sigma_{j=1}^{N} m u_j$, must not change with the number of SPAM particles N for the same flow. Thus, U is ''nonextensive'' with respect to N, and the Boltzmann constant must be rescaled with $1/N$ for such systems). Also the force parameter s is set equal to unity, and Lucy's weight function (11) is used. Our reference system consists of $N = 2500$ SPAM particles of mass $m = 1$. For other N, the particle mass is rescaled to keep the total mass unchanged. Since only totally condensed drops with no atmosphere are considered, no boundary conditions are required. The range

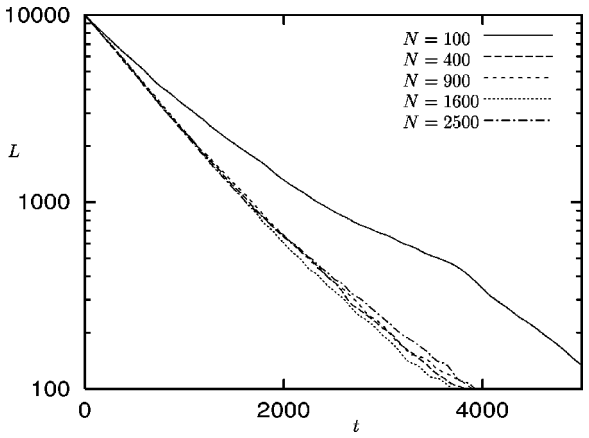

FIG. 9. Time decay of the total angular momentum of a circular drop consisting of N SPAM particles. The smoothing range $h = 15$. Reduced units are used as explained in the Appendix.

h of the weight function (11) is varied between 5 and 15. In all simulations, the initial temperature $T_i = 1$ for all i. For the viscosities we use $\eta = 5$ and $\eta_v = 1$. The heat conductivity is set to $\kappa = 5$. Such a large value is chosen to reduce temperature gradients, but we have verified that our results are totally insensitive to the choice of this parameter.

First, an equilibrated circular drop with vanishing angular momentum is prepared, similar to that depicted in Fig. 1(a). Next, this drop is rotationally accelerated with an external torque (equal for each particle with respect to the center of mass), until a threshold for $\mathbf{L}$ is reached, which is still far below the stability threshold of the circular drop. In the final stage of the simulation, the decay of the angular momentum is followed. In two dimensions, there is only one nonvanishing component, $L(t)$. In Fig. 9 we find an almost exponential decay of $L(t)$ for various systems with identical smoothing length, $h = 15$, and with particle numbers varying between 2500 and 100. With the exception of the too-coarsely-grained case $N = 100$, the decay curves do not depend on N. Thus, the particle error ϵ_N mentioned in the Introduction is insignificant. It should be noted that due to mass rescaling all curves in Fig. 9 refer to drops with about the same diameter and density. If the physical size of the drops were increased

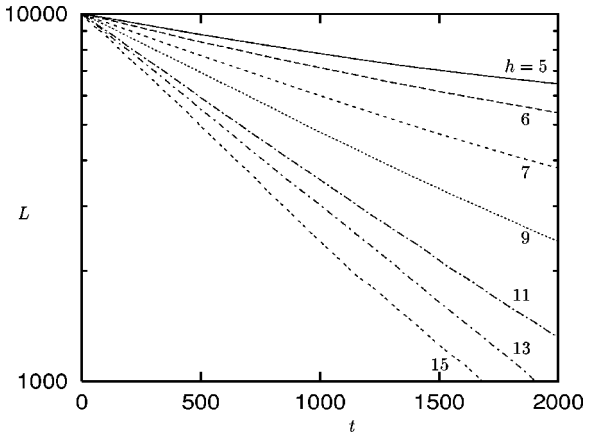

FIG. 10. Time decay of the total angular momentum of a circular drop consisting of 900 SPAM particles. The smoothing range h is indicated by the labels. Reduced units are used as explained in the Appendix.

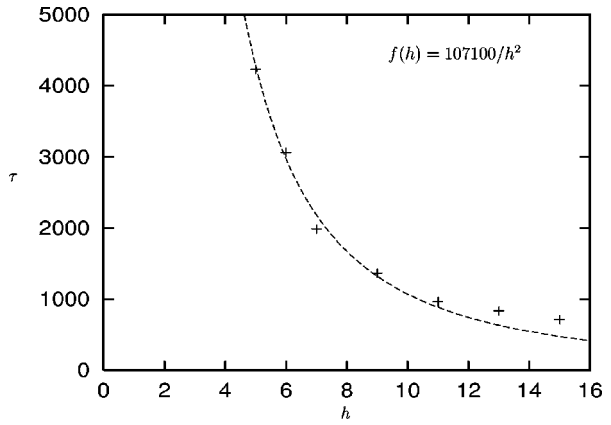

FIG. 11. The time constant τ for the angular momentum decay of a circular drop with 900 SPAM particles as a function of the smoothing length h. The dashed line is a fit of c/h^2 to the data points with $c=107\,100$. Reduced units are used as explained in the Appendix.

by increasing N *without* rescalation of the particle mass, and keeping h constant, the decay time for **L** would increase and the conservation failure become less severe.

In Fig. 10 we compare the decay of $L(t)$ for a system containing 900 SPAM particles, all of mass $m=2.778$, for various smoothing ranges h. The relaxation times τ, defined by $L(t)\propto\exp(-t/\tau)$, are shown in Fig. 11 as a function of h. The dashed line is a fit of $\tau=c/h^2$ to the data points, where the fit parameter $c=1.1\times10^5$ is insensitive to N. This demonstrates that angular momentum decay is indeed of second order in h as expected from the theoretical considerations of Sec. I. Angular momentum is conserved only to order $O(h)$, if a full Newtonian stress tensor is used. We have also verified that the decay time τ is strictly proportional to $1/\eta$ as suggested by Eq. (A2).

In conclusion, numerical simulations demonstrate that the interpolation error inherent to the discrete SPAM representation of continuous fields causes an error of order h^2 for the time derivative of the total angular momentum. For closed systems the angular momentum decays to zero exponentially with a time constant independent of N, for large enough N.

We have mentioned in Sec. II that the equations of motion (4) and (5) are not unique. We computed the angular momentum decay also for the motion equations used by Riffert *et al.* [11], a form of the equations that treat the density differently, and obtained very similar results. This demonstrates that the results in this appendix are insensitive to the particular SPAM representation and are of general interest.

[1] J.C. Brackbill, D.B. Kothe, and C. Zemach, J. Comput. Phys. **100**, 335 (1992).
[2] J.J. Monaghan, Applied Mathematics Reports and Reprints 95/44, Monash University, 1995.
[3] J.P. Morris, Int. J. Numer. Methods Fluids **33**, 333 (2000).
[4] L.B. Lucy, Astron. J. **82**, 1013 (1977).
[5] J.J. Monaghan, Annu. Rev. Astron. Astrophys. **30**, 543 (1992).
[6] W.G. Hoover, T.G. Pierce, C.G. Hoover, J.O. Shugart, C.M. Stein, and A.L. Edwards, Comput. Math. Appl. **28**, 155 (1994).
[7] H.A. Posch, W.G. Hoover, and O. Kum, Phys. Rev. E **52**, 1711 (1995).
[8] *Advances in the Free-Lagrange Method*, edited by H.E. Trease, M.J. Fritts, and W.P. Crowley, Lecture Notes in Physics Vol. 395 (Springer-Verlag, Berlin, 1991).
[9] W. Benz, in *The Numerical Modelling of Nonlinear Stellar Pulsations: Problems and Prospects*, Vol. 302 of *NATO Advanced Study Institute Ser. C*: edited by J.R. Buchler (Kluwer, Dordrecht, 1990), p. 269.
[10] P. Laguna, Astrophys. J. **439**, 814 (1995).
[11] H. Riffert, H. Herold, O. Flebbe, and H. Ruder, Comput. Phys. Commun. **89**, 1 (1995).
[12] O. Kum and W.G. Hoover, J. Stat. Phys. **76**, 1075 (1994).
[13] Wm. G. Hoover, Physica A **260**, 244 (1998).
[14] O. Kum, W.G. Hoover, and H.A. Posch, Phys. Rev. E **52**, 4899 (1995).
[15] H.A. Posch and W.G. Hoover, Physica A **240**, 286 (1997).
[16] J. van der Waals, thesis, Leiden, 1873 [cited by M. Kac, G.E. Uhlenbeck, and P. Hemmer, J. Math. Phys. **4**, 216 (1963)].
[17] J.L. Lebowitz and O. Penrose, J. Math. Phys. **7**, 98 (1966).
[18] J.S. Rowlinson and B. Widom, *Molecular Theory of Capillarity* (Clarendon Press, Oxford, 1982).
[19] N.G. Hadjiconstantinou, A.L. Garcia, and B.J. Alder, Physica A **281**, 337 (2000).
[20] J.P. Hunter, Ph.D. thesis, Monash University, Melbourne, 1992.
[21] S. Nugent, Ph.-D. thesis, University of Vienna, 1998.
[22] L.D. Landau and E. M. Lifshitz, *Statistical Physics* (Pergamon Press, Oxford, 1959), Vol. 5.
[23] B.J. Alder and W.G. Hoover, in *Physics of Simple Liquids*, edited by H.N.V. Temperley, J.S. Rowlinson, and G.S. Rushbrooke (North-Holland, Amsterdam, 1968), p. 79.
[24] A. Elsner, Phys. Lett. A **156**, 147 (1991).
[25] Lord Rayleigh, Proc. R. Soc. London **29**, 71 (1879).
[26] C. M. Stein, Ph.D. thesis, University of California at Davis, 1998.
[27] R.E. Apfel, Y. Tian, J. Jankovsky, T. Shi, X. Chen, R.G. Holt, E. Trinh, A. Croonquist, K.C. Thornton, A. Sacco, Jr., C. Coleman, F.W. Leslie, and D.H. Matthiesen, Phys. Rev. Lett. **78**, 1912 (1997).
[28] H. Takeda, S.M. Miyama, and M. Sekiya, Prog. Theor. Phys. **92**, 939 (1994).